

# GPR H-PLANE ANTENNA PATTERNS FOR A HORIZONTAL DIPOLE ON A HALF-SPACE INTERFACE

Stanley J. Radzevicius and Jeffrey J. Daniels

The Ohio State University, Department of Geological Sciences, 275 Mendenhall Laboratory, 125 S. Oval Mall, Columbus, OH 43210, USA

radzev@geology.ohio-state.edu, jdaniels@geology.ohio-state.edu

Chi-Chih Chen

The Ohio State University, Electroscience Laboratory, 1320 Kinnear Road  
Columbus, OH 43212, USA

ccc@brewster.eng.ohio-state.edu

## ABSTRACT

GPR dipole antenna patterns can be described by the interference of space and lateral waves. Because this is an interference phenomenon, antenna patterns are a function of frequency, distance, and electrical properties. Traditional far-field criteria based on dipoles in a whole-space are insufficient to describe dipole antennas on a half-space boundary. Whole-space criteria fail because they do not take into account the interference of space and lateral waves. The travel time difference between space and lateral waves increases as the angle of observation from vertical increases, or with increasing distance from the source. The result is increased interference and more abundant lobes with increasing distance and observation angle.

Since GPR investigations are limited by attenuation and many environmental and engineering targets of interest are located within a few wavelengths of the antenna, asymptotic solutions do not accurately describe antenna patterns for most GPR applications. The exclusion of lateral waves in geometric optics solutions is another source of error for many GPR applications. Data were measured over a water filled tank to verify FDTD antenna pattern models. Asymptotic solutions predict H-plane peaks at an angular distance equal to the critical angle. Measured and modeled antenna patterns are broader and have peaks located at a larger angular distance, than predicted from asymptotic solutions. The peaks approach and decrease the rate of convergence toward the asymptotic solution with increasing distance from the source, and data modeled over water demonstrate that the peaks still do not converge to the asymptotic solution at a distance of 24 wavelengths. The low directivity of dipole antennas explains why out of the plane reflections are commonly observed in GPR data.

Key words: antenna patterns, H-plane, half-space, horizontal dipole antennas, space waves, lateral waves

## INTRODUCTION

Understanding the radiation pattern of dipole antennas near a planar boundary between two semi-infinite media has been an important subject for ground penetrating radar (GPR) research and applications. Sommerfeld developed asymptotic far-field solutions for a Hertzian dipole as early as 1909. Norton applied Sommerfeld theory to engineering applications dealing with the propagation of radio waves over the surface of the earth and in the upper atmosphere (1936, 1937a, 1937b). Baños (1966) worked on the conductive seawater-air interface at low frequencies in which the conduction currents are greater than the displacement currents. Baños, using asymptotic integral solutions, divided the antenna pattern into three regions: 1) near-field, 2) intermediate field, and 3) asymptotic far field. The boundaries between these three regions are described in terms of wavenumber ratios between the two materials. Further work on antennas over a half-space can be found in many other publications (Wait, 1962; Annan, 1973; King *et al.*, 1974; Annan *et al.*, 1975; Sorbello *et al.*, 1977; Engheta *et al.*, 1982; Smith, 1984; Arcone, 1995). The advent of faster computers in the 1990's made numerical modeling of antenna patterns feasible (Wensink *et al.*, 1990; Roberts and Daniels, 1994; Turner, 1994; Holliger and Bergmann, 1998).

All of the asymptotic integral techniques require assumptions to find an analytical solution. Many of these assumptions are not valid for GPR applications. The targets of interest in GPR surveys are often located in the near-field of the antenna and actual antenna patterns can be significantly different than the patterns described by asymptotic far-field solutions that include

only geometric optics (GO) terms. Displacement currents dominate many GPR applications and solutions based on assumptions of high conductivity are not appropriate. This paper investigates antenna patterns through numerical modeling and physical measurements. Because most GPR data are collected with antennas located on or near the ground, this paper focuses on dipole antennas located on a half-space interface. The H-plane applies directly to the most common mode of GPR data acquisition, in which the transmit and receive antennas are oriented parallel to each other and orthogonal to the survey direction (broadside mode). An understanding of the mechanisms responsible for producing the H-plane pattern also provides insight into other antenna pattern cross-sections. It is the intent of this paper to provide a better understanding of the physical mechanisms that produce antenna patterns.

## EXPERIMENTAL SETUP AND MEASUREMENTS

Experiments were conducted to verify calculated results from numerical models. Measurements were conducted over a fluid because it is homogeneous and because it allowed easy movement of probing targets and antennas in the lower half-space. The probing target was moved at a constant radius and thus eliminated the need for attenuation and spreading corrections. A  $10^\circ$  bow-tie antenna located on an air-water interface (Figure 1) was used as the antenna under test (AUT). A cylindrical polyethylene tank having a height of 1.2 m and a diameter of 2.4 m was filled with tapwater characterized by a relative dielectric permittivity  $\epsilon_r = 80$  and conductivity  $\sigma = .027$  S/m at 60 MHz.

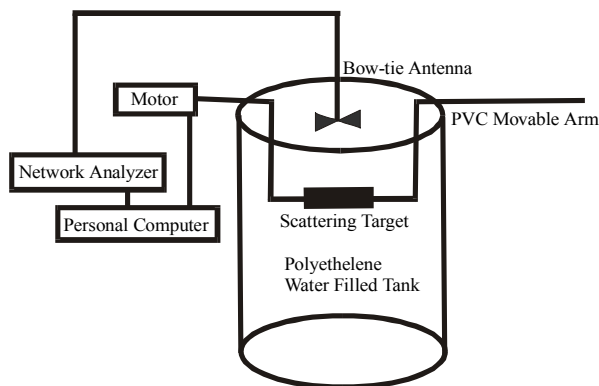


Figure 1 : Experimental setup for measuring antenna patterns over water filled tank.

A moveable arm constructed of PVC pipe drilled with holes to allow water to enter the portion of the structure that was submerged, and thus lower its radar cross section, served as the supporting structure for the scattering

target. The radiation pattern was determined from backscattering measurements, where a probing target was used to generate the backscattered fields. Compared to the direct probing technique that uses a field probing antenna, no cable is present to cause measurement error. The probing target consisted of a thin rectangular conducting plate. The probing target orientation with respect to the AUT was constant. This eliminated the need for probe pattern correction except at large angles (near interface) where the coupling between the interface and probe became significant. Measurements were conducted with several other targets such as metallic spheres, and metallic tape wrapped about the PVC support structure, and similar antenna pattern results were obtained. The conducting plate gave the strongest signal level and resulted in the best signal-to-noise ratio among the probing targets tested. A swept-frequency network analyzer was used to transmit and receive the electromagnetic signals via the AUT. A personal computer was used to record data and control the motor and network analyzer that recorded data at  $1^\circ$  increments up to  $5^\circ$  below the air-water interface.

The network analyzer and feed cable were calibrated by adding a short, open, and matched load to the end of the feed cable. A background measurement with no target present was later used in processing to remove scattering from the tank walls and water surface. Range gate was also applied to isolate interactions between the probing target and the tank. The data were then Fourier transformed back into the frequency domain so that antenna patterns could be computed for each frequency.

## FINITE DIFFERENCE TIME DOMAIN MODELING

Finite difference time domain (FDTD) modeling was performed to investigate the physical mechanisms that produce antenna patterns for horizontal dipole antennas located on air-ground interfaces. An infinite line source was used to approximate the H-plane of dipole antennas. A Gaussian pulse was used as the excitation signal for the line source at time = 0. It was observed that there are two mechanisms, the space waves (direct and reflected) and the lateral waves. Figure 2 shows a snap shot of the calculated result at time = 15 ns over water having a relative dielectric permittivity of 81 and conductivity of 0 S/m. The wavefront of the lateral wave is inclined at an angle equal to the critical angle with respect to the half-space interface. For a half-space characterized by  $\epsilon_r=81$  and  $\sigma = 0$  S/m, the critical angle ( $\theta_c \approx 6^\circ$ ) is given by  $\text{asin}(1/\sqrt{\epsilon_r})$  for a lossless, non-magnetic material. The wavefronts for the space and

lateral waves would appear spherical and conical in three-dimensions.

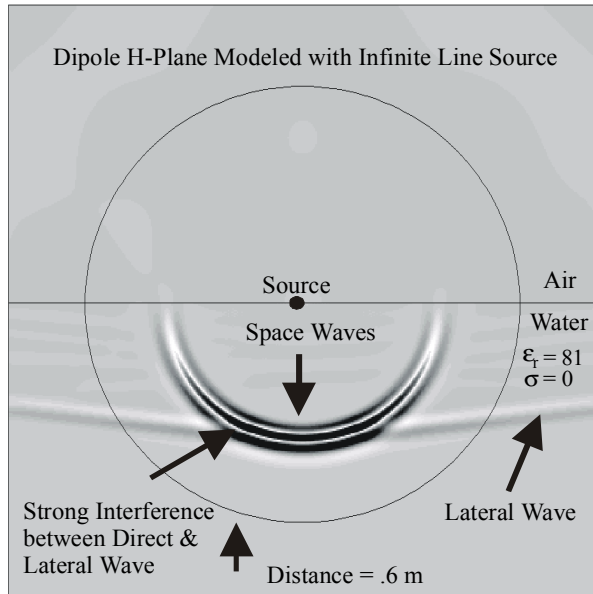


Figure 2: Snap shot of the FDTD calculated fields for an infinite line source located on an air-water interface ( $\epsilon_r = 81$ ,  $\sigma = 0$  S/m). The wavefronts of the space and lateral waves are clearly visible.

Figure 3 compares normalized FDTD and measured antenna patterns at a distance equal to 2 wavelengths in water. The peaks of the measured and modeled patterns agree and are observed at approximately  $30^\circ$ . Constructive interference between direct and lateral waves is responsible for producing these peaks. The side lobes observed in the modeled data are not present in the measured data. This discrepancy may be caused by measurement error near the interface produced by strong coupling between the probe and interface. Figure 4 compares the pattern obtained from the FDTD simulation at a distance of 8 wavelengths (solid) with that predicted from far-field asymptotic integral solutions (dash-dot). The asymptotic solutions represent the geometric optics solution for the fields and thus does not contain the lateral wave component. The interference between the direct and lateral waves gives rise to the lobed structures in the antenna patterns and explains the lack of side lobes in the GO solution. The radiation peaks predicted from the FDTD simulation slowly converge and approach the  $6^\circ$  location predicted by the far-field solution as distance increases (compare Figures 3 and 4). By a distance of 24 wavelengths, the peaks are located at approximately  $15^\circ$ , but still have not reached the critical angle, as predicted by GO asymptotic solutions.

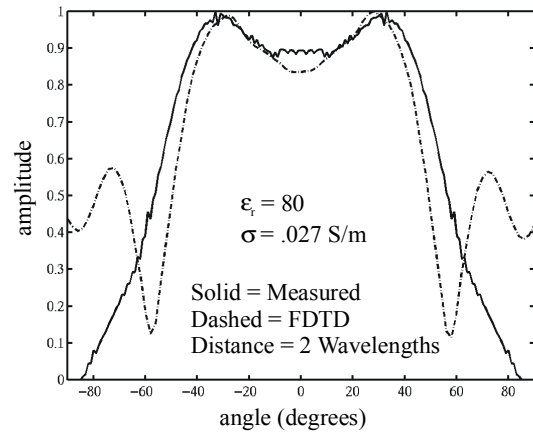


Figure 3: Comparison of measured (solid) and FDTD calculated (dashed-dot) normalized antenna patterns at a distance of 2 wavelengths in water ( $f = 100$  MHz,  $\epsilon_r = 80$ ,  $\sigma = .027$  S/m).

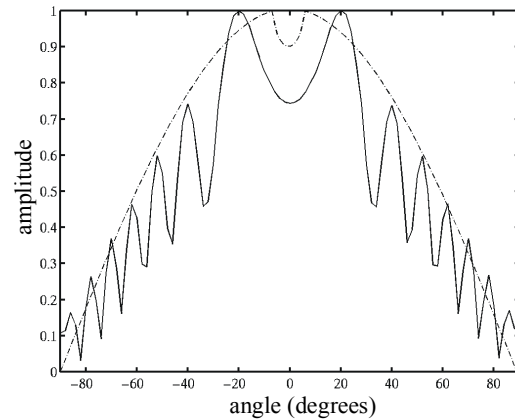


Figure 4: Comparison of GO asymptotic solution (dashed-dot) and FDTD (solid) at a distance of 8 wavelengths in water ( $f = 100$  MHz,  $\epsilon_r = 81$ ,  $\sigma = 0$  S/m).

The lobes in the FDTD model are caused by the interference of the direct and lateral waves. The number and amplitude of lobes is determined by the relative amplitude and phase difference of the direct and lateral wave components. The number of lobes increases with increasing distance from the source and increased observation angle because of increased phase difference between the direct and lateral waves under these conditions (observation angle is measured from vertical and equals  $\pm 90^\circ$  at the interface). The lateral wave phase front is characterized by  $k_d L_o + k_o L_1 + k_d L_2 = \text{constant}$ , and is inclined with respect to the interface by an angle

equal to the critical angle (Figures 2 and 5), where  $k$  denotes wavenumber.

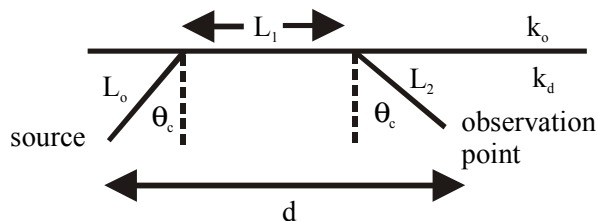


Figure 5: Propagation geometry for lateral waves.

Lateral waves are attenuated less than space waves in lossy materials. The total travel path of space waves is confined to the lossy medium while the lateral waves travel from the transmit antenna to the surface through the lossy medium and then propagate in air with little attenuation to the receive antenna. Lateral wave amplitudes are characterized by  $d^{-1/2}L_1^{-3/2}$  for a point source and show caustic behavior in the neighborhood of  $L_1 \rightarrow 0$  (Brekhovskikh, 1980). This is in contrast to guided surface waves with spreading confined to two dimensions and thus characterized by a  $1/\sqrt{r}$  spreading factor. Where  $d$  = lateral distance between source and observation point and  $r$  = radial distance. The lateral wave is evanescent and decays exponentially away from the interface in the upper air half-space. Increased attenuation of lateral waves relative to space waves is observed in FDTD models for lossy media.

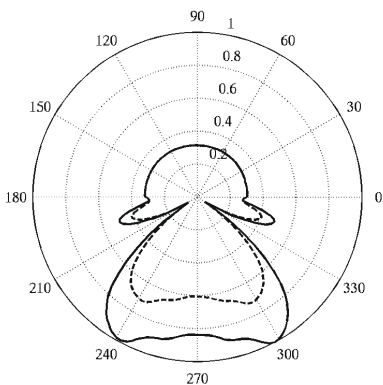


Figure 6: FDTD normalized polar antenna pattern plot at a distance of 2 wavelengths in water for  $\epsilon_r = 81$  and  $\sigma = 0$  S/m (solid),  $\sigma = .027$  S/m (dashed) [0-180° air, 180-360° water].

The effects of electrical properties on antenna patterns are illustrated in Figures 6 and 7. Figure 6 is a normalized polar plot that compares antenna patterns at a dis-

tance of 2 wavelengths for water having a permittivity of 81 and conductivities of 0 and .027 S/m respectively. Fields radiated into the ground relative to the air weaken with increases in subsurface conductivity. Decreasing the relative dielectric permittivity from 81 to 7 causes the critical angle to increase from approximately 6° to 22°. This results in broader main lobes as shown in Figure 7. Radiation into the air is also reduced by increases in the dielectric permittivity of the subsurface.

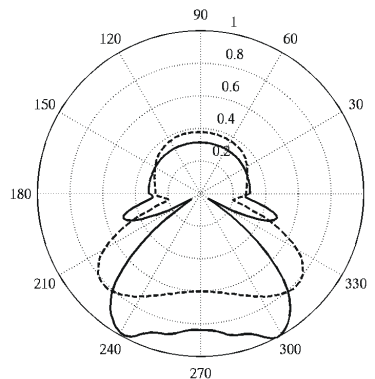


Figure 7: FDTD normalized polar antenna pattern plot at a distance of 2 wavelengths in water for  $\sigma = 0$  S/m and  $\epsilon_r = 81$  (solid),  $\epsilon_r = 7$  (dashed) [0-180° air, 180-360° soil].

## CONCLUSIONS

This manuscript has investigated H-plane antenna patterns for horizontal dipoles located on half-space interfaces. This is useful for GPR because most GPR surveys are conducted in broadside mode with antennas located on or near the ground. FDTD techniques provide a useful tool to understand broad-band width GPR antenna radiation properties as long as the distance of interest is not too large to pose computation problems. The measurement setup proved to be useful for determining the radiation pattern of dipole GPR antennas in the presence of a homogeneous liquid such as water. The measured H-plane pattern agrees well with that predicted by the FDTD model. The FDTD model allows for the computation of antenna patterns for materials having different electrical properties. Radiation into the air relative the soil is reduced by increases in dielectric permittivity. The directivity of antenna patterns also increases with increases in dielectric permittivity.

In general, GPR antenna patterns can be characterized by the interference of space and lateral waves. The space wave term is the geometric optics term and is composed of a direct wave originating at the position of the transmit antenna and a reflected wave that appears to originate from the image of the transmit antenna and

modified by the Fresnel reflection coefficient. It is the interference between these direct and lateral waves that produces the lobes observed in antenna patterns. The interference of direct and lateral wavefronts is clearly visible in FDTD models. Because this is an interference phenomenon, antenna patterns are a function of frequency and depth of investigation.

The lateral wave can be the dominant term in lossy materials because of its shorter travel path through the lossy half-space compared to space waves. The presence of lateral waves makes it impractical to apply the asymptotic solutions to most GPR applications. H-plane patterns for a dipole tend to be broader and thus less directive in most GPR applications than predicted by GO solutions. The majority of H-plane energy is not radiated directly below the antenna, but occurs to the side. Low directivity explains why out of the plane reflections are commonly observed in GPR data. This property is useful for target detection but is not useful for accurately locating targets. The broad antenna patterns demonstrate why migration and 3D GPR surveys are necessary to accurately locate buried objects with dipole antennas.

## REFERENCES

- Annan, A.P., 1973, Radio interferometry depth sounding: Part 1- theoretical discussion, *Geophysics*, Vol. 38, No. 3, pp. 557-580.
- Annan, A.P., Waller, W.M., Strangway, D.W., Rossiter, J.R., Redman, J.D., and Watts, R.D., 1975, The electromagnetic response of a low-loss, 2-layer, dielectric earth for horizontal electric dipole excitation, *Geophysics*, Vol. 40, No. 2, pp. 285-298.
- Arcone, S.A., 1995, Numerical studies of the radiation patterns of resistively loaded dipoles, *Journal of Applied Geophysics*, Vol. 33, pp. 39-52.
- Baños, A., 1966, Dipole radiation in the presence of a conducting half-space, *Pergamon*, New York.
- Brekhovskikh, L.M., 1980, Waves in layered media, *Academic Press*, New York.
- Engheta, N., Papas, C.H., and Elachi, C., 1982, Radiation patterns of interfacial dipole antennas, *Radio Science*, Vol. 17, No. 6, pp. 1557-1566.
- Holliger, K., and Bergmann, T., 1998, Accurate and efficient FDTD modeling of ground-penetrating radar antenna radiation, *Geophysical Research Letters*, Vol. 25, pp. 3883-3886.
- King, R.W.P., Wu, T.T., and Shen, L.C., 1974, The horizontal wire antenna over a conducting or dielectric half-space: Current and admittance, *Radio Science*, Vol. 9.
- Norton, K.A., 1936, The propagation of radio waves over the surface of the earth and in the upper atmosphere: Part 1- Ground wave propagation from short antennas, *Proceedings of the Institute of Radio Engineers*, Vol. 24, No. 10, pp. 1367-1387.
- Norton, K.A., 1937a, The physical reality of space and surface waves in the radiation field of radio antennas, *Proceedings of the Institute of Radio Engineers*, Vol. 25, No. 9, pp. 1192-1202.
- Norton, K.A., 1937b, The propagation of radio waves over the surface of the earth and in the upper atmosphere: Part 2- The propagation from vertical, horizontal, and loop antennas over a plane earth of finite conductivity, *Proceedings of the Institute of Radio Engineers*, Vol. 25, No. 9, pp. 1203-1236.
- Roberts, R., and Daniels, J., 1994, Finite-difference time-domain forward modeling of GPR data, *Proceedings of the Fifth International Conference on Ground Penetrating Radar*, Vol. 1, pp. 185-203.
- Smith, G., 1984, Directive properties of antennas for transmission into a material half-space, *IEEE Transactions on Antennas and Propagation*, Vol. 32, No. 3, pp. 232-246.
- Sommerfeld, A., 1909, Über die ausbreitung der wellen in der drahtlosen telegraphie, *Annalen der Physik*, Vol. 28, pp. 665-737.
- Sorbello, R.M., King, R.W.P., Lee, K.M., Shen, L.C., and Wu, T.T., 1977, The horizontal wire antenna over a dissipative half-space: Generalized formula and measurements, *IEEE Transactions on Antennas and Propagation*, Vol. 25.
- Turner, G., 1994, Modeling antenna-ground interactions, *Proceedings of the Fifth International Conference on Ground Penetrating Radar*, Vol. 1, pp. 205-221.

Wait, J., 1962, Electromagnetic waves in stratified media, *Pergamon*, New York.

Wensink, W.A., Greeuw, G., Hofman, J., and Van Deen, J.K., 1990, Measured underwater near-field E-patterns of a pulsed, horizontal dipole antenna in air: Comparison with the theory of the continuous wave, infinitesimal electric dipole, *Geophysical Prospecting*, Vol. 38, pp. 805-830.